MJO-related oceanic Kelvin waves and the ENSO cycle: A study with the NCEP Global Ocean Data Assimilation System

Kyong-Hwan Seo[1] and Yan Xue[2]

[1] The surface wind anomalies associated with the Madden-Julian oscillation (MJO) appear to play a critical role during the onset and termination phases of ENSO. The characteristics of the MJO-related oceanic Kelvin waves have not been systematically studied due to a lack of ocean reanalysis that resolves intraseasonal variability. This study uses the operational ocean reanalysis for the period 1982–2003 produced by the state-of-art global ocean data assimilation system at NCEP to explore the relationship between SST anomalies of ENSO and MJO-related oceanic Kelvin waves. The first four extended empirical orthogonal functions of the depth of 20°C isotherm are used to represent the dominant oceanic Kelvin waves. The wave activity is measured by seasonal variance of oceanic Kelvin waves (SVKW) at 130°W. SVKW peaks are associated with the onset stage of warm ENSO events since they occur during the transition period and tend to produce positive tendency in NINO3.4 and heat content, and lead mature phases by 5–11 months. MJO-related oceanic Kelvin wave activity is also shown to impact the growth and termination of warm events. The consistent relationships do not occur in cold events. A real time monitoring tool using SVKW index is proposed to support the official ENSO forecast at NCEP. **Citation:** Seo, K.-H., and Y. Xue (2005), MJO-related oceanic Kelvin waves and the ENSO cycle: A study with the NCEP Global Ocean Data Assimilation System, *Geophys. Res. Lett.*, *32*, L07712, doi:10.1029/2005GL022511.

1. Introduction

[2] There is some evidence that oceanic Kelvin waves associated with the Madden-Julian oscillation (MJO) play a critical role during the onset and termination phases of ENSO [*Kessler et al.*, 1995; *McPhaden*, 1999; *Bergman et al.*, 2001]. Here we attempt to investigate the relationship between SST anomalies of ENSO and MJO-related oceanic Kelvin waves using the pentad ocean reanalysis for 1979–2004 produced by the global ocean data assimilation system (GODAS) at the National Environmental Prediction Center (NCEP) [*Behringer and Xue*, 2004].

[3] Understanding how MJO activity affects ENSO is difficult due to a number of factors. Firstly, using a global measure of MJO activity, *Hendon et al.* [1999] found that MJO activity and ENSO are essentially uncorrelated at zero lag. However, *Zhang and Gottschalck* [2002] and *Lau*

[2005] showed that seasonal variance of Kelvin wave forcing and MJO activity precedes mature phase of ENSO. Secondly, modeling results are also controversial. *Zebiak* [1989] showed that, in a simple model, effects of the atmospheric intraseasonal variability on ENSO are small. However, *Kessler and Kleeman* [2000] suggested the presence of the MJO amplified SST anomalies by ~50% during the 1997/98 event through rectification to low-frequency variations. Thirdly, the physical mechanism for the MJO-ENSO interaction is not clearly understood. This is probably due to the fact that most coupled models for ENSO do not simulate the MJO realistically.

[4] The linkage between the ENSO cycle and oceanic Kelvin wave activity has not been systematically studied due to the scarcity of high-frequency subsurface ocean data. In this study, this relationship is explored using the NCEP Optimum Interpolation (OI) SST analysis [*Reynolds et al.*, 2002] and ocean reanalysis from NCEP. Oceanic Kelvin wave activity is measured by seasonal variance of the depth of 20°C isotherm anomalies at 130°W. It will be shown that peaks of this index are associated with the onset, growth and termination of ENSO warm events.

2. GODAS Data

[5] The GODAS was developed using the Geophysical Fluid Dynamics Laboratory Modular Ocean Model version 3 (MOM.v3) and a three-dimensional variational data assimilation scheme [*Behringer and Xue*, 2004]. It utilizes the momentum flux, heat flux and fresh water flux from the NCEP reanalysis 2 [*Kanamitsu et al.*, 2002], and assimilates temperature and synthetic salinity that is constructed from temperature and local T-S (temperature-salinity) climatology. The temperature data includes those from XBTs, profiling floats and TAO (Tropical Atmosphere Ocean) moorings.

[6] Figure 1 shows the time series of pentad temperature from the GODAS and TAO observations at the depth of 120 meters at the mooring site 0°N and 140°W. Although TAO observations show a sharper variation, the GODAS temperature is in relatively good agreement with the TAO data and gives us confidence in using the GODAS data to study the intraseasonal oceanic variability. In this study, we only use the GODAS for 1982–2003 since the NCEP OI SST used in this work starts in 1982. Also, due to sparse data distribution and poor wind forcing in the early 1980s, we do not include the 1982/83 ENSO event in our study.

3. EEOF of Depth of 20°C Isotherm

[7] An extended empirical orthogonal function (EEOF) analysis is applied to the intraseasonally filtered (20–120 days) depth of 20°C isotherm (D20) anomalies averaged

---

[1]RSIS/Climate Prediction Center, NCEP/NWS/NOAA, Camp Springs, Maryland, USA.
[2]Climate Prediction Center, NCEP/NWS/NOAA, Camp Springs, Maryland, USA.
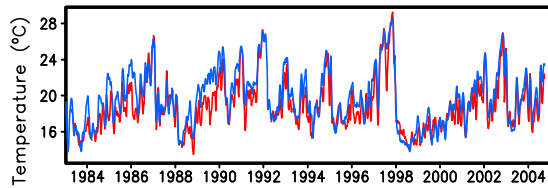
Figure 1. Pentad temperature (°C, 3-point-running mean) at the TAO mooring site 140°W, 0°N and at the depth of 120 meters. TAO observations (red) and GODAS (blue).

over 2°S–2°N for 1982–2003. A recursive filter is used here since it produces realistic ending values, suitable for a real time implementation [*Rasmusson et al.*, 1994]. In the EEOF analysis, we use 20 lagged pentads to capture the dominant period of oceanic Kelvin waves. The first (second) pair of EEOFs accounts for 39% (13%) of the variance, and their principal components (PCs) have a lag correlation of 0.95 (0.90) at 4 pentads (3 pentads), describing eastward propagating oceanic Kelvin waves at a period of ~80 days (~60 days, respectively). The first two EEOF pairs are well separated from each other and higher order modes according to the criteria of *North et al.* [1982]. Figure 2 shows the lagged correlation coefficients of the filtered equatorial D20 and zonal wind stress anomalies with the first PC (PC1) and third PC (PC3). It is seen in Figure 2a that the downwelling Kelvin wave (contour) begins to develop near 140°E where the westerly wind forcing (shading) exhibits a maximum amplitude, and propagates eastward, reaching a maximum correlation of ~0.8 near 130°W when the eastward propagating easterly wind anomaly catches up with the downwelling Kelvin wave. The corresponding correlation with the zonal wind
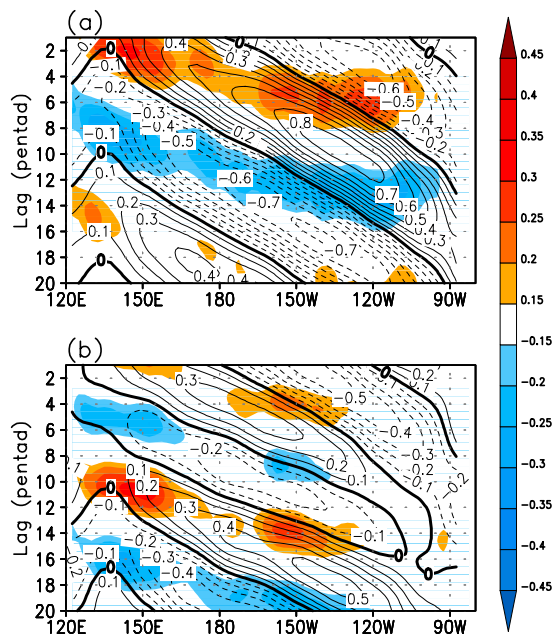
Figure 2. Lagged correlation of filtered D20 (contours) and zonal wind stress (shading) anomalies averaged from 2°S to 2°N for the (a) first and (b) third principal components of the EEOFs. The contour interval is 0.1 with the zero contour thickened.
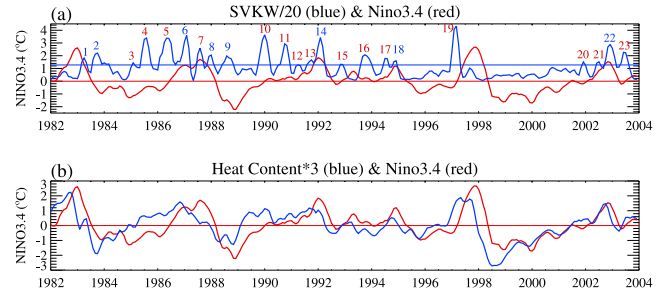

Figure 3. Comparison of seasonal NINO3.4 anomalies (red) with (a) the SVKW index (blue), (b) the seasonal HC index (blue). HC index is the average temperature in the top 300 meters along the equatorial belt between150°E–100°W, 5°S–5°N. Units for SVKW and HC are scaled to fit to that of NINO3.4 in °C. A total of 23 isolated maximum SVKW events that exceed 0.2 standard deviations (thin blue line) are labeled in Figure 3a. Downwelling (upwelling) Kelvin wave packets are denoted as red (blue) color.

stress is much smaller (~0.3). For the PC3, the relationship between D20 and zonal wind stress is similar to that for the PC1 except the period is shorter. For D20, its correlation with the PC3 is much smaller than that with the PC1. But for the zonal wind stress, its correlation with the PC1 and PC3 are comparable. It is noticed that the eastward propagation of zonal wind stress of PC3 is not as clear as that of PC1. The current analysis tends to support the previous study of *Hendon et al.* [1998] that the oceanic Kelvin waves selectively respond to the low-frequency tail of intraseasonal wind variations related to the MJO.

4. Relationship Between ENSO and Seasonal Variance of Oceanic Kelvin Waves

[8] On the seasonal time scale, the envelope of oceanic Kelvin waves (wave packet) is often used to describe wave activity [*Kessler et al.*, 1995]. In this study, the oceanic Kelvin waves are represented by the D20 anomalies reconstructed from the first four EEOFs. The magnitude of the wave packet is estimated using the seasonal variance of oceanic Kelvin waves (SVKW) (i.e., the averaged pentad variance within running 90-day windows) at 130°W where the wave activity is largest. It is shown in Figure 3a along with NINO3.4 index (SST average in 170°W–120°W, 5°S–5°N). Here, a total of 23 isolated SVKW peaks having amplitude greater than 0.2 standard deviations are identified. Each SVKW peak represents a Kelvin wave packet that can be distinguished as either positive (downwelling) or negative (upwelling) wave packet by consulting the total D20 anomalies averaged in a season. This takes account of the fact that intraseasonal Kelvin waves are embedded in the low-frequency background thermocline variations and their impacts on D20 over a season are indistinguishable from those from the low-frequency variations. The total D20 anomalies are the real physical quantity that influences SST. So the seasonal average of total (unfiltered) D20 anomalies for the region [150°E–120°W, 2°S–2°N] centered at the calendar month of each SVKW peak is calculated, and its sign determines whether the wave packet is a positive or negative packet. Since some of Kelvin
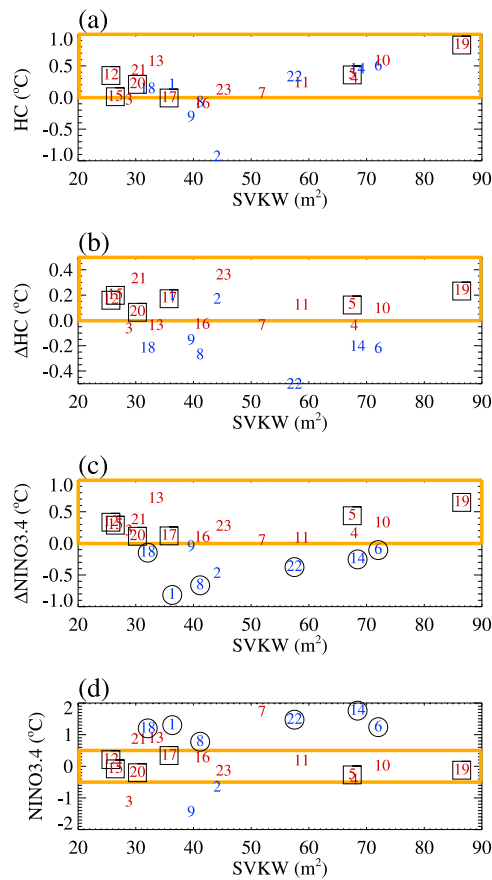
Figure 4. The 23 isolated maximum SVKW values from Figure 3a plotted against (a) the seasonal HC index, (b) HC tendency, (c) NINO3.4 tendency, and (d) the seasonal NINO3.4 index. Tendency is calculated with the difference $T(t + 1) - T(t - 1)$ centered at the calendar month (t) of each event. The yellow rectangles denote the regions for onset candidate. The six black squared positive SVKW values correspond to the onset phase of 1986/87, 1991/92, 1993, 1994/95, 1997/98 and 2002/03 warm events. The six black circled negative SVKW events correspond to the termination phase.

waves are only present in the eastern Pacific, the seasonal average of total D20 anomalies for the region [160°W–100°W, 2°S–2°N] is additionally calculated and this helps identify events 5 and 16 in Figure 3a as downwelling Kelvin wave packets. The above procedure results in 15 downwelling and 8 upwelling Kelvin wave packets (Figure 3a). Figure 3b shows the seasonal heat content (HC) index.

[9] Figure 4 shows the scatter plots for the 23 isolated SVKW peaks vs. HC, NINO3.4 and their respective tendency. It is seen in Figure 4a that the HC index is biased positive, and tends to be linearly proportional to SVKW when SVKW is greater than 40 m² regardless of the sign of the Kelvin wave packets (positive labeled as red and negative labeled as blue). The HC tendency shows some degree of separation between downwelling and upwelling packets (Figure 4b). About 70% of the former (latter) events identified give rise to an increase (decrease) of HC. It is quite interesting to see the change of NINO3.4

index due to the presence of the Kelvin wave packets (Figure 4c). All downwelling (upwelling) Kelvin wave packets lead to an increase (decrease) in the NINO3.4 index and this reveals a rather clear relationship between the oceanic Kelvin wave packet and the development of rectified low-frequency variations in the NINO3.4 region. The rectification in the SST anomalies by downwelling Kelvin wave packets is particularly effective when NINO3.4 is small (Figure 4d). Interestingly, most of downwelling wave packets occur during the transition phase while most of upwelling wave packets occur during the peak phase of warm ENSO events (Figure 4d).

[10] Among the 11 downwelling wave packets whose NINO3.4 indices are between -0.5 and $0.5°C$, the SVKW peaks 5, 12, 15, 17, 19 and 20 (marked as a square in Figure 4 and dated in May 1986, April 1991, November 1992, July 1994, March 1997 and December 2001, respectively) are associated with the six El Niños in 1986/87, 1991/92, 1993, 1994/95, 1997/98 and 2002/03. The time interval between each SVKW peak and the mature phase of its corresponding warm event varies from 5 to 11 months. They are also characterized by a positive HC and positive tendency of HC and NINO3.4.

[11] Not all the SVKW peaks whose NINO3.4 is within -0.5 and $0.5°C$ lead to warm ENSO events as in SVKW peaks 4, 10, 11, 16 and 23 (Figure 4d). The peaks 4 and 16 (August 1985 and October 1993) have a negative SST average over the western Pacific, and the tendency of NINO3.4 and HC are small. The peak 10 dated in January 1990 is particularly interesting since SVKW, HC and NINO3.4 tendency are quite large and most of the ENSO models produced a false warm event in 1991. However, as the trade winds intensified in May 1990, SST anomalies in the central and east Pacific weakened and convective activity moved to west of the date line [Bergman et al., 2001]. The peak 11 (October 1990) has a rather small increase in NINO3.4 and after this event, the NINO3.4 index falls in the following winter and spring seasons. The peak 23 (June 2003) satisfied our onset criteria, but this
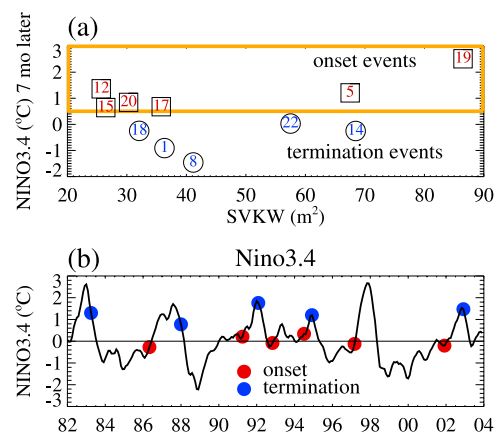
Figure 5. (a) SVKW and NINO3.4 index in seven months for onset and termination events. Event 6 has been omitted due to an increase of the NINO3.4 index in 1987 June. (b) Time series of seasonal NINO3.4 anomalies (black) and six onset events (marked by red circles) and five termination events (marked by blue circles).

resulted in warm SST anomalies in NINO3.4 region for only four consecutive overlapping seasons. Since the peaks 11 and 23 occur in fall and summer, they do not have enough time to grow before the winter decay season arrives.

[12] Kelvin wave activity also influences the growth and termination phases of warm ENSO events. Downwelling wave packets 13 and 21 appear to amplify the SST anomalies in the NINO3.4 region in relation to the 1991/92 and 2002/03 El Niños. Meanwhile, at the height of the warm ENSO events, upwelling Kelvin wave packets appear (events 1, 6, 8, 14, 18, and 22 marked as a circle in Figure 4) and tend to reduce the SST anomalies. Seven months after the passage of the upwelling Kelvin wave packets, the NINO3.4 index becomes negative as shown in Figure 5a. Therefore, the oceanic Kelvin waves play an important role in the whole evolution of an ENSO warm event. The downwelling Kelvin wave packet helps set up the onset stage and intensify the SST anomalies over the Pacific during the developing phase, and the upwelling Kelvin wave packet tends to accelerate the termination of a warm event. Figure 5b summarizes the characteristics.

5. Discussion and Conclusions

[13] The relationship between ENSO and MJO-related oceanic Kelvin wave activity measured by the seasonal variance of oceanic Kelvin waves (SVKW) at 130°W is explored. Although the overall lag correlation between SVKW and NINO3.4 index is only 0.23, SVKW peaks are related to the onset stage of the warm ENSO events since they tend to occur when NINO3.4 is close to zero, and induce positive tendency in NINO3.4 and heat content, and lead mature phases of ENSO by 5–11 months. SVKW peaks are also related to the growth and termination of warm ENSO events.

[14] For the six SVKW peaks leading to warm ENSO events, the NINO3.4 index in 7 months seems to be proportional to the amplitude of the SVKW (Figure 5a). Although the correlation coefficient calculated is ~0.8, it is heavily dependent on the 1997/98 case (peak 19). If that case is excluded, there appears no significant relationship between these two variables. The similar conclusion emerges when NINO3.4 at their respective peak ENSO phase is used.

[15] It seems that both enhanced Kelvin wave activity and positive HC are precursory signal for the development of warm events (Figure 4a). However, this is not the case for cold events. In fact, the Markov model based mainly on sea level (equivalent to heat content) forecasts cold events reasonably well, but underestimates warm events [*Xue et al.*, 2000]. This may be because the oceanic Kelvin wave

signal is excluded from the Markov model. The proper inclusion of oceanic Kelvin wave activity in statistical and numerical models for ENSO may improve forecast skill but it remains a challenging task. At the present, we propose to use the SVKW index as a real time monitoring tool to support the official ENSO forecast at NCEP.

References

Behringer, D., and Y. Xue (2004), Evaluation of the global ocean data assimilation system at NCEP: The Pacific Ocean, paper presented at Eighth Symposium on Integrated Observing and Assimilation Systems for Atmosphere, Ocean, and Land Surface, Am. Meteorol. Soc., Seattle, Wash.

Bergman, J. W., H. H. Hendon, and K. M. Weickmann (2001), Intraseasonal air-sea interactions at the onset of El Niño, *J. Clim.*, *14*, 1702–1719.

Hendon, H. H., B. Liebmann, and J. D. Glick (1998), Oceanic Kelvin waves and the Madden-Julian Oscillation, *J. Atmos. Sci.*, *55*, 88–101.

Hendon, H. H., C. Zhang, and J. D. Glick (1999), Interannual variability of the Madden-Julian Oscillation, *J. Clim.*, *12*, 2538–2550.

Kanamitsu, M., W. Ebisuzaki, J. Woollen, S.-K. Yang, J. J. Hnilo, M. Fiorino, and G. L. Potter (2002), NCEP-DOE AMIP-II Reanalysis (R-2), *Bull. Am. Meteorol. Soc.*, *83*, 1631–1643.

Kessler, W. S., and R. Kleeman (2000), Rectification of the Madden-Julian Oscillation into the ENSO cycle, *J. Clim.*, *13*, 3560–3575.

Kessler, W. S., M. J. McPhaden, and K. M. Weickmann (1995), Forcing of intraseasonal Kelvin waves in the equatorial Pacific, *J. Geophys. Res.*, *100*, 10,613–10,631.

Lau, K.-M. (2005), El Niño Southern Oscillation–climate connections, in *Intraseasonal Variability in the Atmosphere-Ocean Climate System*, edited by K.-M. Lau and D. E. Waliser, Springer, New York.

McPhaden, M. J. (1999), Genesis and evolution of the 1997–98 El Niño, *Science*, *283*, 950–954.

North, G. R., T. L. Bell, R. F. Cahalan, and F. J. Moeng (1982), Sampling errors in the estimation of empirical orthogonal functions, *Mon. Weather Rev.*, *110*, 699–706.

Rasmusson, E. M., X. L. Wang, and C. F. Ropelewski (1994), Secular variability of the ENSO cycle, in *Decade to Century Time Scales of Natural Climate Variability*, 630 pp., Elsevier, New York.

Reynolds, R. W., N. A. Rayner, T. M. Smith, D. C. Stokes, and W. Wang (2002), An improved in situ and satellite SST analysis for climate, *J. Clim.*, *15*, 1609–1625.

Xue, Y., A. Leetmaa, and M. Ji (2000), ENSO prediction with Markov model: The impact of sea level, *J. Clim.*, *13*, 849–871.

Zebiak, S. E. (1989), On the 30–60 day oscillation and the prediction of El Niño, *J. Clim.*, *2*, 1381–1387.

Zhang, C., and J. Gottschalck (2002), SST anomalies of ENSO and the Madden-Julian Oscillation in the equatorial Pacific, *J. Clim.*, *15*, 2429–2445.

———————

K.-H. Seo, Climate Prediction Center, NCEP/NWS/NOAA, Room 806, WWB, 5200 Auth Road, Camp Springs, MD 20746, USA. (kyonghwan.seo@noaa.gov)

Y. Xue, Climate Prediction Center, NCEP/NWS/NOAA, Rm. 605-A, WWB, 5200 Auth Road, Camp Springs, MD 20746, USA.